Diindenoperylene thin-film structure on MoS$_2$ monolayer

N. Mrkyvkova,[1,2,a] M. Hodas,[3] J. Hagara,[1] P. Nadazdy,[1] Y. Halahovets,[1] M. Bodik,[1,4] K. Tokar,[1,4] J. W. Chai,[5] S. J. Wang,[5] D. Z. Chi,[5] A. Chumakov,[6] O. Konovalov,[6] A. Hinderhofer,[3] M. Jergel,[1] E. Majkova,[1,2] P. Siffalovic,[1,2] and F. Schreiber[3]

AFFILIATIONS

[1]Institute of Physics, Slovak Academy of Sciences, Dúbravská cesta 9, Bratislava 84511, Slovakia
[2]Centre of Excellence for Advanced Materials Application, Dúbravská cesta 9, Bratislava 84511, Slovakia
[3]Institut für Angewandte Physik, Universität Tübingen, Auf der Morgenstelle 10, 72076 Tübingen, Germany
[4]Advanced Technologies Research Institute, Faculty of Materials Science and Technology in Trnava, Slovak University of Technology in Bratislava, 917 24 Trnava, Slovakia
[5]Institute of Materials Research & Engineering (IMRE), A*STAR (Agency for Science, Technology and Research), 2 Fusionopolis Way, Innovis, Singapore 138634
[6]European Synchrotron Radiation Facility, 71 avenue des Martyrs, Grenoble 38000, France

[a]Author to whom correspondence should be addressed: nada.mrkyvkova@savba.sk

ABSTRACT

Research on two-dimensional (2D) atomic crystals is one of the highly progressive topics in (opto)electronics, as the van der Waals (vdW) interactions enable integration of 2D crystals with a broad range of materials. Organic π-conjugated molecules offer new opportunities for creating the so-called "hybrid" vdW heterostructures, in which their anisotropy adds an extra degree of functional possibilities. Moreover, it was found that in the case of organic molecules, the 2D substrate changes the molecular orientation, which in turn can enhance the overall optoelectronic properties. However, the reorientation of the molecules has been until now studied solely on the graphene underlayer that restrained its applicability to a broader range of materials. Here, we study the molecular orientation of diindenoperylene (DIP), a representative of rodlike organic semiconductors, on the MoS$_2$ monolayer. Our results show that DIP forms separate islands on the top of the MoS$_2$ monolayer with lying-down orientation of the molecules. We combine the grazing-incidence X-ray diffraction technique with atomistic simulations to reveal the exact molecular arrangement on the atomically thin underlayer. We also investigate optical absorption spectra for different thicknesses of the DIP layer, as they are of fundamental importance for various applications in organic-based optoelectronics.

Published under license by AIP Publishing. https://doi.org/10.1063/1.5100282

The common feature of small organic molecules to self-assemble into a crystal on a solid surface is one of the key parameters for their use in different organic-based applications. Most aromatic molecules are anisotropic, and the resulting optical and electrical properties of crystalline organic thin films are anisotropic as well.[1–3] In order to optimize the efficiency of molecule-based devices, the molecular orientation in the film has to be controlled for each application. For example, in horizontal organic field effect transistors (OFETs), the maximum (in-plane) charge-carrier mobility is normally obtained for vertical (standing-up) orientation of the molecules.[4,5] Nevertheless, this orientation is detrimental for vertical OFETs[6,7] or organic solar cells, where the highest light absorption is achieved when the molecular long axis is parallel to the electric field vector, which in practice means a lying-down orientation of molecules.[3,4,6,8] The molecular orientation, morphology, and thus the (opto)electronic properties of such organic layers depend on the intermolecular interaction between the deposited molecules and the interfacial molecule-substrate interactions.[3,9] The lying-down (λ) orientation is observed for strongly interacting substrates, such as metals.[3,10–13] However, on inert substrates, like oxides, which are suitable for thin-film transistors or for organic photovoltaics, a majority of molecules adopt a standing-up (σ) orientation.[8,14,15] It is because the van der Waals (vdW) interactions with neighboring molecules are energetically more favorable compared to the relatively weak interactions with the substrate.[9] It was recently demonstrated that the two-dimensional (2D) template layer of graphene deposited on weakly interacting substrates changes the molecular orientation from standing-up to lying-down.[1,2,7,16] Introducing the inorganic 2D interlayer enables creating the so-called hybrid (organic/

inorganic) vdW heterostructures. This might bring a wealth of novel applications by taking advantage of 2D layers with various electrical properties and the virtually infinite degrees of freedom offered by the design of organic molecules.[6,17–22]

In this letter, we report on the crystalline structure and molecular packing of diindenoperylene (DIP), a representative organic semiconductor, on the MoS$_2$ monolayer. Unlike semimetallic graphene, MoS$_2$ belongs to the group of transition metal dichalcogenides (TMDC). It is a direct bandgap semiconductor with a bandwidth of 1.88 eV for a monolayer.[23] The nontrivial bandgap features make MoS$_2$ a great candidate to push forward many photonic and electronic devices that are currently based on bulk III–V and IV semiconducting materials.[24] DIP was chosen because of its promising properties, e.g., the ambipolar behavior with high charge mobilities[25] and long exciton diffusion length in thin films.[26] So far, thin layers of DIP have been studied on various substrates, including Si/SiO$_2$,[14,27] Au,[3,10,11,28] rubrene,[14,27] Cu,[13] etc. It was observed that the self-organization of DIP in thin films is different from that of the bulk crystal.[29] The unit cell (UC) of thin films was found to be very similar to the high-temperature (HT) phase of the bulk crystal even for the temperatures lower than 423 K, where the phase transition occurs in the bulk.[25,29,30] Furthermore, the coexistence of σ and λ orientations was reported, and their relative ratio was assigned to the film thickness and the substrate temperature.[10,30,31] Despite the extensive number of studies on DIP thin films, the complete structure including the molecular arrangement remains unknown. Combining grazing-incidence wide-angle X-ray scattering (GIWAXS) with theoretical calculations, we were able to determine the crystallographic unit cell of the DIP thin film and the spatial arrangement of the molecules on the MoS$_2$ monolayer. This detailed study of DIP ordering in the vdW heterostructures will broaden the knowledge of their (opto)electronic properties, which in turn might be helpful for the proper design and utilization in future devices.

The MoS$_2$ monolayer was grown on c-plane Al$_2$O$_3$ substrates by the one-step process, using magnetron sputtering of the Mo target in vaporized sulfur ambience. This technique leads to a good quality monolayer or few-layer MoS$_2$ films on a wafer scale. The Al$_2$O$_3$ substrate was precleaned using acetone in an ultrasonic bath prior to placing it into the deposition chamber. The growth was carried out at a substrate temperature of 700 °C and a sulfur partial pressure of 4.0×10^{-7} mbar. The processing gas (Ar) pressure was fixed at 6.0×10^{-4} mbar, and the sputtering power was 6 W. With this low sputtering power, the growth rate was extremely low in order to achieve monolayer growth. The film thickness was checked by Raman spectroscopy [see Fig. 1(a)]. The Raman spectra were measured using

FIG. 1. (a) Raman spectra of the MoS$_2$ monolayer on the sapphire substrate. Two characteristic Raman vibrational modes of MoS$_2$–E$^1_{2g}$ and A$_{1g}$ are labeled. The peak at ~417.9 cm^{-1} is attributed to A$_{1g}$ of the sapphire substrate. (b) AFM image of the DIP crystals on the MoS$_2$ monolayer.

a confocal Raman microscope (Witec, Alpha300 R+) with an excitation wavelength of 523 nm and a scanning area of 30×30 μm^2. DIP was purchased from the Institute of Physics, University of Stuttgart (Stuttgart, Germany), in the powder form. The thin films were prepared in a vacuum chamber by organic molecular beam deposition (OMBD) so that the DIP powder was heated up to 250 °C in an effusion cell and evaporated onto the MoS$_2$ monolayer. Before the actual deposition of DIP, the MoS$_2$/Al$_2$O$_3$ substrate was annealed at 320 °C in order to desorb any unfavorable surface contamination. The substrate was subsequently cooled down, and its temperature was kept constant at 50 °C during the deposition. The vacuum base pressure was below 2×10^{-8} mbar, and the deposition nominal rate was ~1.0 Å/min (monitored in real time using a quartz crystal microbalance). We note that the deposition rate is inferred from the DIP growth on a Si wafer, where the molecules adopt the standing-up orientation. The subsequent ex $situ$ thickness calibration of DIP on Si was performed by spectroscopic ellipsometry (J.A. Woolam, M-2000V) utilizing the tabulated values of n and k parameters.[32] The morphology of the DIP films was studied by atomic force microscopy (Bruker, Dimension Edge) in the tapping mode. The GIWAXS measurements were performed at the ESRF–ID10 beamline (Grenoble, France), where the synchrotron X-ray radiation energy was tuned to 9.25 keV and the angle of incidence (α_i) was set to 0.2°. The deposition chamber was equipped with a 360° cylindrical beryllium window, enabling the detection of wide-angle diffractions. The intensity of the diffracted beam was detected using an area detector Pilatus 300K (Dectris) with a 320 μm thick Si sensor. The detector allowed us to monitor the in-plane ($q_{||}$) as well as the out-of-plane ($q_{\perp}$) components of diffraction spots simultaneously with a quantum efficiency of 95%. We also measured the ex $situ$ optical absorption of the thin films for various DIP thicknesses. The absorption spectra were obtained from the transmission measurements performed using a Lambda 950 UV/Vis spectrophotometer (PerkinElmer) at room temperature.

To obtain the arrangement of DIP molecules within the unit cell, the initial parameters taken from the high-temperature bulk structure[33] were put into the experimentally determined unit cell on the MoS$_2$ underlayer. We optimized the atomic positions with respect to the ground state energy minimum of the system while keeping the unit cell parameters fixed. For the optimization, we employed the density-functional theory (DFT) in generalized-gradient approximation (GGA) along with the projector augmented-wave (PAW) approach[34] as implemented in the VASP simulation package.[35] The $4 \times 3 \times 2$ k-point Monkhorst-Pack mesh and an energy cutoff of 500 eV for the plane wave basis set were chosen in the calculations of the electronic system. We described the vdW interaction by DFT-D2 Grimme's correction term.[36] The structures were converged with tolerances of 10^{-7} eV and 10^{-5} eV for electronic and ionic degrees of freedom, respectively.

Figure 1(a) shows the Raman spectra in the vicinity of the characteristic Raman vibrational modes for MoS$_2$–E$^1_{2g}$ and A$_{1g}$,[37,38] which were obtained as an average of the scans within the probed area. The frequency difference between E$^1_{2g}$ and A$_{1g}$ modes is ~20 cm^{-1}, confirming a monolayer of MoS$_2$.[39,40] Furthermore, we also observed the photoluminescence of the MoS$_2$ layer, which is strong in the case of the monolayer and direct bandgap semiconductor but quickly decays for an indirect bandgap multilayer.[23] Figure 1(b) shows the AFM images of the DIP layer with an effective thickness of 12 nm, revealing an islandlike shape of the crystals. We note that in order to reasonably
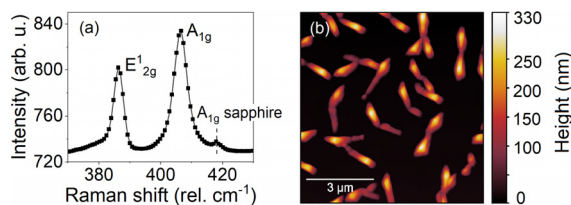
denote the DIP thickness on the MoS_2 underlayer, we use the term "effective thickness," which indicates the thickness of the DIP film grown on the Si wafer with a thin native oxide layer (Si/SiO_2). The reason is that in the case of 2D substrates—like graphene or MoS_2—the molecules form isolated islands after being deposited on the surface (Volmer-Weber growth mode),[16] whereas on Si/SiO_2, a layer-by-layer growth takes place and persists up to 7–8 monolayers, i.e., up to ~13 nm.[14,41] The use of the effective thickness even for discontinuous films formed of islands is thus more straightforward and comprehensible.

The different morphology on bulk substrates like Al_2O_3, Si, or ITO[8,41–43] compared to the MoS_2 monolayer indicates that the molecular orientation may also be different. The islandlike shape of the DIP crystals is similar to the arrangement of the various rodlike molecules on graphene, where the molecules adopt the lying-down orientation.[1,7,16,19,44] In order to determine the orientation of DIP on the MoS_2 monolayer, we employed additional experimental studies and theoretical calculations which are described below.

Figure 2 shows the GIWAXS reciprocal space map of the 12 nm thick DIP film. The diffraction spots shown in Fig. 2 were visible regardless of the azimuthal orientation of the sample, which points to isotropic crystallographic orientation of the DIP crystallites in the substrate plane, forming the so-called fiber texture.[30,45] This indicates that the MoS_2 substrate is not just one monocrystal, but rather it is formed of many randomly oriented monocrystalline regions. Furthermore, Fig. 2 documents that all diffractions are doubled. As the angle of the incident beam ($\alpha_i = 0.20°$) was very close to the critical angle of the underlying substrate ($\alpha_c^{MoS_2} = 0.27°$), the reflection and refraction effects have to be taken into account.[45] These effects act exclusively on the $q_\perp$ components, which explains the observed Bragg spot duplicity along $q_\perp$. The lower peak from each doublet represents a direct diffraction of the incident X-ray beam in the DIP layer. On the other hand, the upper peak arises as a combination of the total reflection of the beam from the MoS_2 substrate (as the angle of incidence of the refracted beam in the DIP layer is smaller than $\alpha_c^{MoS_2}$) and the subsequent Bragg diffraction in the organic film. Consequently, both peaks carry information about the crystal structure, but the upper one also encodes the reflectivity of the
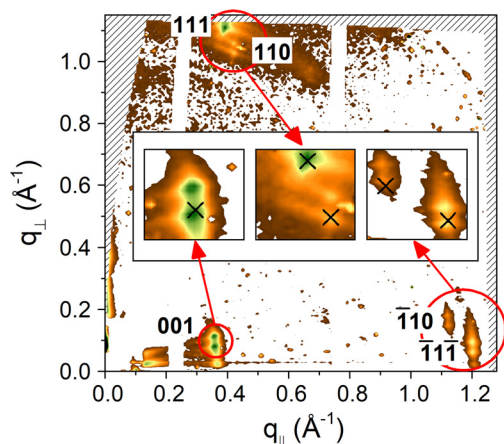
substrate. Therefore, we will concentrate only on the lower diffractions and omit the redundant information embedded in the upper peaks. We note that we have also performed a refraction correction for the lower diffraction peaks.[45] The resulting shift of the peak positions in the $q_\perp$ direction was not significant, and its influence on the determined unit cell parameters was only within the experimental error.

In order to calculate the DIP thin film unit cell (UC) dimensions, we used the genetic algorithm (GA) optimization procedure in Matlab. Assuming that the UC will be close to the high-temperature (HT) bulk phase, we were able to index the observed diffraction peaks as 001, $\bar{1}$10, $\bar{1}1\bar{1}$, 110, and 111. The reciprocal positions ($q_\parallel$ and $q_\perp$) of these diffraction spots were subsequently used as constraints in the GA optimization. Until now, the HT bulk phase was considered to sufficiently describe the arrangement of DIP molecules in the thin films[29,30] However, the theoretical peak positions calculated for the HT unit cell did not match our experimental data for any spatial orientation of the UC. Moreover, the monoclinic HT unit cell belongs to the space group No. 14 [P2$_1$/c] and the symmetry of this group does not allow the 001 diffraction. We found that the UC parameters obtained by the GA are similar to the ones of the HT bulk phase[33]— see Table I, but the crystal space group is triclinic [No. 2, ($P\bar{1}$)]. The different thin film structure might originate from the lattice mismatch between the organic layer and the substrate. This mismatch leads to stress during the growth, causing structural transitions.[46]

We note that the GA not only provides the information about the parameters of the UC but also calculates its orientation with respect to the substrate, as will be discussed later in the text. Theoretical positions of the diffraction peaks, inferred from the determined UC parameters, are shown in Fig. 2. It can be seen that they are in good agreement with the measured diffractions.

In order to roughly estimate the spatial orientation of the molecules, we can utilize the position of the 001 diffraction. From the magnitude of the q_{001}-vector, we can obtain the lattice spacing d_{001} along the reciprocal UC vector c^*. The lattice spacing $d_{001} = (16.9 \pm 0.3)$ Å indicates that the directions of the molecule's long axis (18.4 Å) and the crystallographic c-axis are nearby. Thus, the spatial orientation of the 001 diffraction, pointing along the $q_\parallel$ direction [with only a slight tilt of ~12.7° (see Fig. 2)], suggests that the molecules are oriented along the substrate plane, i.e., in the λ-orientation.

With the unit cell dimensions and orientation established, we now turn to the molecular orientations on MoS_2. The equilibrium molecular positions were calculated by the DFT described earlier in this manuscript. The herringbone arrangement of the molecules within the unit cell is defined by a commonly used set of angles[47,48] (see Fig. 3) as follows. The angle between c^* and the molecular long axis is denoted by χ. The mutual angle between two molecular long axes is δ, and θ is the herringbone angle, i.e., the angle between the molecular short axes. The calculated angles for the two molecules inside the experimentally determined unit cell are $\chi_1 = 18.80°$, $\chi_2 = 19.01°$, $\delta = 3.49°$, and $\theta = 59.40°$. The exact orientation of the molecules within the UC enables a visualization of their arrangement on the MoS_2 monolayer since the orientation of the UC can be determined by the GA from the GIWAXS data, as quoted earlier. The UC orientation is given by the vector $s = (a \cdot \sin \psi \cdot \cos \varphi, b \cdot \sin \psi \cdot \sin \varphi, c \cdot \cos \psi)$, where the angles ψ and φ are the initial parameters in the GA optimization (together with the UC parameters a, b, c, α, β, and γ) and s is the normal to the substrate plane, see Fig. 3(b). The calculated

FIG. 2. The q-space map of the 12 nm thick DIP layer on the MoS_2 monolayer (intensity increasing from brown to green). The 001, $\bar{1}$10, $\bar{1}1\bar{1}$, 110, and 111 diffraction peaks are magnified for a better resolution. The black crosses indicate the calculated positions of the diffraction peaks, using the determined unit cell parameters.

TABLE I. Unit cell parameters of the thin-film phase and the high-temperature bulk phase.

	a (Å)	b (Å)	c (Å)	α (°)	β (°)	γ (°)
Thin film	7.26 ± 0.02	9.04 ± 0.03	17.08 ± 0.03	87.3 ± 0.3	91.3 ± 0.2	88.3 ± 0.2
Bulk crystal[33]	7.17	8.55	16.80	90.0	92.4	90.0

tilt angle between the molecular long axes and the substrate plane is $\eta_1 = 1.46°$ and $\eta_2 = 4.48°$ for the first and the second molecule in the UC, respectively, which can be considered as a direct confirmation of the lying-down (λ) orientation of the molecules. It is also interesting to mention that the calculated angle between the c^*-axis and the substrate plane is 11.19°. This value is in good agreement with the experimentally determined spatial orientation of the 001 diffraction from the GIWAXS data (12.7°).

Furthermore, we investigated the optical properties of DIP thin films, as they are generally less thoroughly investigated compared to electrical or structural properties and as they are directly coupled to the geometrical structure.[50] The optical absorption spectra are of fundamental importance for different applications in organic-based optoelectronics. Figure 4 shows the absorption spectra measured for DIP layers with different thicknesses, together with the bare MoS_2 monolayer as a reference. The MoS_2 excitonic peaks A and B at 1.88 eV and 2.02 eV are clearly visible, and their spectral position confirms a good quality of the MoS_2 monolayer.[49] Moreover, the absorption spectra exhibit at least two other distinguishable features, which can be attributed to the transitions from the highest occupied molecular orbitals (HOMOs) to the lowest unoccupied molecular orbitals (LUMOs), i.e., the intramolecular HOMO–LUMO transitions, with a vibronic progression of $\Delta E \sim 0.17$ eV. The spectral positions of these peaks are $E_{00} = 2.25$ eV and $E_{01} = 2.42$ eV, which are visible already from the DIP thickness of ~ 1 nm. We note that the position of the E_{00} peak is shifted for the DIP film deposited on the MoS_2 monolayer compared to the optical response of the DIP monomer ($\Delta E_{00} = 0.1$ eV).[32] The red-shift in absorption in the crystalline thin films was explained by the formation of Frenkel excitons and their interference with charge transfer states.[32,51] Typically, in the energy range shown in Fig. 4 (1.6–2.9 eV), at least three peaks of the vibronic progression of the π–π^* transition were previously observed.[32,52] In our case, the third peak of the vibronic progression at $E_{02} \sim 2.6$ eV starts to appear at a thickness of 12 nm, but for the thinner layers, the energetically higher peaks are most likely suppressed by the background absorption originating from the Al_2O_3/MoS_2 substrate. The gradual increase in the π–π^* transition intensity with the increasing DIP thickness is evident. It can be explained by the fact that the molecular transition dipole moment (for transitions around 2.25 eV) is oriented along the long axis.[32] Since the DIP molecules (and thus the molecular long axis) are oriented almost within the substrate plane, the oscillatory strength (i.e., the absorption cross section) increases with the increasing DIP thickness, when taking into account the normal incidence of light employed in the experiment. The same character of the absorption spectra was also observed for PTCDA (3,4,9,10-Perylentetracarbonsäuredianhydrid), which typically adopts the lying-down configuration on different substrates.[53] On the other hand, we did not observe a spectral mode that was reported by Heinemeyer et al.[50] for the standing-up DIP molecules as a consequence of the intermolecular coupling.
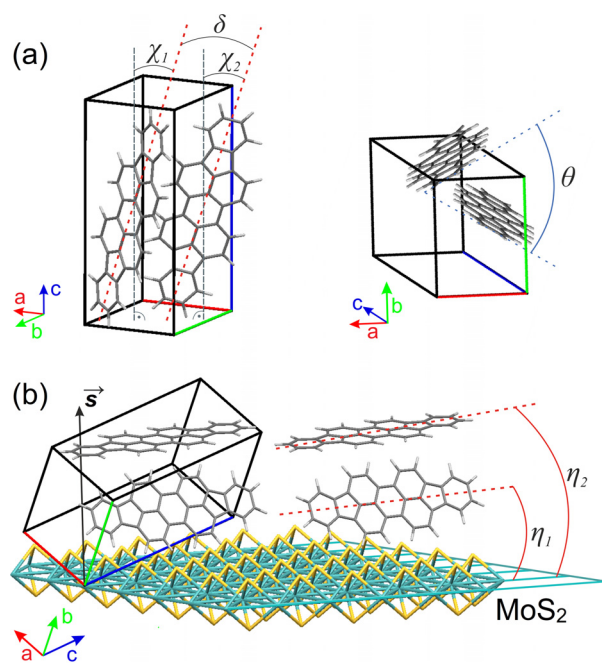
FIG. 3. (a) Orientation of DIP molecules within the UC characterized by a set of angles. χ_1, χ_2 are the angles between the molecular long axes (red dashed line) and c^* (gray dashed line), δ is the mutual angle between the molecular long axes, and θ is the herringbone angle between the molecular short axes. (b) The UC orientation on the MoS_2 monolayer is given by the vector **s**, and the tilt of the molecular long axes with respect to the substrate is given by the angles η_1 and η_2.
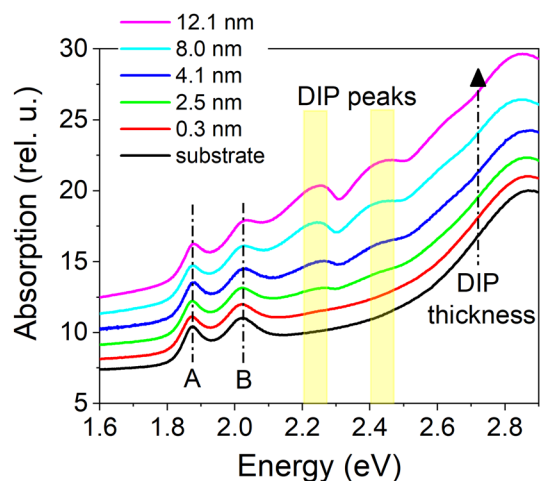
FIG. 4. Absorption spectra of DIP layers with different thicknesses grown on the MoS_2 monolayer. A and B denote the excitonic transition bands for the MoS_2 monolayer at 1.88 eV and 2.02 eV, respectively.[49] Absorption spectra are vertically shifted for clarity.

In conclusion, we have studied the morphology and molecular orientation of DIP thin films on the MoS$_2$ monolayer. Employing the GIWAXS technique, we were able to solve the crystal structure of the thin film phase, confirming its close resemblance to the high temperature bulk structure. On the other hand, we found out that the DIP crystal space group is triclinic on the MoS$_2$ monolayer, which is in contrast to the recently reported monoclinic structure of DIP on silicon substrates.[30] Moreover, we went beyond determination of the common lattice parameters. We performed theoretical DFT calculations, which enabled solving the DIP crystal structure with the exact molecular arrangement and the atomic positions within the UC. The presented combination of the experimental and computational methods can also be applied to other molecules that create highly ordered crystals on 2D underlying layers. Determination of the molecular orientation is especially important in organic (opto)electronics, where the properties such as the charge-carrier lifetime, interfacial energetics, or the light absorption are strongly correlated with the anisotropic nature of molecules.[1,2,7]

REFERENCES

[1] S. B. Jo, H. H. Kim, H. Lee, B. Kang, S. Lee, M. Sim, M. Kim, W. H. Lee, and K. Cho, ACS Nano **9**, 8206 (2015).

[2] W. H. Lee, J. Park, S. H. Sim, S. Lim, K. S. Kim, B. H. Hong, and K. Cho, J. Am. Chem. Soc. **133**, 4447 (2011).

[3] C. Schünemann, D. Wynands, K. J. Eichhorn, M. Stamm, K. Leo, and M. Riede, J. Phys. Chem. C **117**, 11600 (2013).

[4] J. Roncali, P. Leriche, and A. Cravino, Adv. Mater. **19**, 2045 (2007).

[5] F. Liscio, C. Albonetti, K. Broch, A. Shehu, S. D. Quiroga, L. Ferlauto, C. Frank, S. Kowarik, R. Nervo, A. Gerlach, S. Milita, F. Schreiber, and F. Biscarini, ACS Nano **7**, 1257 (2013).

[6] M. Gobbi, E. Orgiu, and P. Samorì, Adv. Mater. **30**, 1706103 (2018).

[7] I. Salzmann, A. Moser, M. Oehzelt, T. Breuer, X. Feng, Z. Y. Juang, D. Nabok, R. G. Della Valle, S. Duhm, G. Heimel, A. Brillante, E. Venuti, I. Bilotti, C. Christodoulou, J. Frisch, P. Puschnig, C. Draxl, G. Witte, K. Müllen, and N. Koch, ACS Nano **6**, 10874 (2012).

[8] L. Zhang, S. S. Roy, N. S. Safron, M. J. Shearer, R. M. Jacobberger, V. Saraswat, R. J. Hamers, M. S. Arnold, and T. L. Andrew, Adv. Mater. Interfaces **3**, 1600621 (2016).

[9] T. Tian and C.-J. Shih, Ind. Eng. Chem. Res. **56**, 10552 (2017).

[10] A. C. Dürr, N. Koch, M. Kelsch, A. Rühm, J. Ghijsen, R. L. Johnson, J.-J. Pireaux, J. Schwartz, F. Schreiber, H. Dosch, and A. Kahn, Phys. Rev. B **68**, 115428 (2003).

[11] D. G. De Oteyza, E. Barrena, M. Ruiz-Osés, I. Silanes, B. P. Doyle, J. E. Ortega, A. Arnau, H. Dosch, and Y. Wakayama, J. Phys. Chem. C **112**, 7168 (2008).

[12] C. B. France, P. G. Schroeder, and B. A. Parkinson, Nano Lett. **2**, 693 (2002).

[13] H. Aldahhak, S. Matencio, E. Barrena, C. Ocal, W. G. Schmidt, and E. Rauls, Phys. Chem. Chem. Phys. **17**, 8776 (2015).

[14] S. Kowarik, A. Gerlach, and F. Schreiber, J. Phys. Condens. Matter **20**, 184005 (2008).

[15] F. Schreiber, Phys. Status Solidi A **201**, 1037 (2004).

[16] M. Hodas, P. Siffalovic, P. Nádaždy, N. Mrkyvková, M. Bodík, Y. Halahovets, G. Duva, B. Reisz, O. Konovalov, W. Ohm, M. Jergel, E. Majková, A. Gerlach, A. Hinderhofer, and F. Schreiber, ACS Appl. Nano Mater. **1**, 2819 (2018).

[17] D. Jariwala, S. L. Howell, K. S. Chen, J. Kang, V. K. Sangwan, S. A. Filippone, R. Turrisi, T. J. Marks, L. J. Lauhon, and M. C. Hersam, Nano Lett. **16**, 497 (2016).

[18] Y. Huang, F. Zhuge, J. Hou, L. Lv, P. Luo, N. Zhou, L. Gan, and T. Zhai, ACS Nano **12**, 4062 (2018).

[19] T. Breuer, T. Maßmeyer, A. Mänz, S. Zoerb, B. Harbrecht, and G. Witte, Phys. Status Solidi RRL **10**, 905 (2016).

[20] M. Gobbi, S. Bonacchi, J. X. Lian, Y. Liu, X. Y. Wang, M. A. Stoeckel, M. A. Squillaci, G. D'Avino, A. Narita, K. Müllen, X. Feng, Y. Olivier, D. Beljonne, P. Samorì, and E. Orgiu, Nat. Commun. **8**, 14767 (2017).

[21] Z. Zheng, X. Zhang, C. Neumann, D. Emmrich, A. Winter, H. Vieker, W. Liu, M. Lensen, A. Gölzhäuser, and A. Turchanin, Nanoscale **7**, 13393 (2015).

[22] D. Jariwala, T. J. Marks, and M. C. Hersam, Nat. Mater. **16**, 170 (2017).

[23] K. F. Mak, C. Lee, J. Hone, J. Shan, and T. F. Heinz, Phys. Rev. Lett. **105**, 136805 (2010).

[24] Y. Yoon, K. Ganapathi, and S. Salahuddin, Nano Lett. **11**, 3768 (2011).

[25] A. K. Tripathi and J. Pflaum, Appl. Phys. Lett. **89**, 082103 (2006).

[26] D. Kurrle and J. Pflaum, Appl. Phys. Lett. **92**, 133306 (2008).

[27] S. Kowarik, A. Gerlach, S. Sellner, F. Schreiber, L. Cavalcanti, and O. Konovalov, Phys. Rev. Lett. **96**, 125504 (2006).

[28] M. B. Casu, I. Biswas, B. E. Schuster, M. Nagel, P. Nagel, S. Schuppler, and T. Chassé, Appl. Phys. Lett. **93**, 024103 (2008).

[29] A. O. F. Jones, B. Chattopadhyay, Y. H. Geerts, and R. Resel, Adv. Funct. Mater. **26**, 2233 (2016).

[30] S. Kowarik, A. Gerlach, S. Sellner, L. Cavalcanti, O. Konovalov, and F. Schreiber, Appl. Phys. A **95**, 233 (2009).

[31] A. Hinderhofer, T. Hosokai, K. Yonezawa, A. Gerlach, K. Kato, K. Broch, C. Frank, J. Novák, S. Kera, N. Ueno, and F. Schreiber, Appl. Phys. Lett. **101**, 033307 (2012).

[32] U. Heinemeyer, R. Scholz, L. Gisslén, M. I. Alonso, J. O. Ossó, M. Garriga, A. Hinderhofer, M. Kytka, S. Kowarik, A. Gerlach, and F. Schreiber, Phys. Rev. B **78**, 085210 (2008).

[33] M. A. Heinrich, J. Pflaum, A. K. Tripathi, W. Frey, M. L. Steigerwald, and T. Siegrist, J. Phys. Chem. C **111**, 18878 (2007).

[34] P. E. Blöchl, Phys. Rev. B **50**, 17953 (1994).

[35] A. R. Miedema, J. Less-Common Met. **32**, 117 (1973).

[36] S. Grimme, J. Comput. Chem. **27**, 1787 (2006).

[37] Y. Liu, H. Nan, X. Wu, W. Pan, W. Wang, J. Bai, W. Zhao, L. Sun, X. Wang, and Z. Ni, ACS Nano **7**, 4202 (2013).

[38] S.-L. Li, H. Miyazaki, H. Song, H. Kuramochi, S. Nakaharai, and K. Tsukagoshi, ACS Nano **6**, 7381 (2012).

[39] G. Siegel, Y. P. Venkata Subbaiah, M. C. Prestgard, and A. Tiwari, APL Mater. **3**, 056103 (2015).

[40] Y. T. Ho, C. H. Ma, T. T. Luong, L. L. Wei, T. C. Yen, W. T. Hsu, W. H. Chang, Y. C. Chu, Y. Y. Tu, K. P. Pande, and E. Y. Chang, Phys. Status Solidi RRL **9**, 187 (2015).

[41] A. C. Dürr, F. Schreiber, M. Münch, N. Karl, B. Krause, V. Kruppa, and H. Dosch, Appl. Phys. Lett. **81**, 2276 (2002).

[42] X. N. Zhang, E. Barrena, D. G. de Oteyza, and H. Dosch, Surf. Sci. **601**, 2420 (2007).

[43] A. C. Dürr, F. Schreiber, K. A. Ritley, V. Kruppa, J. Krug, H. Dosch, and B. Struth, Phys. Rev. Lett. **90**, 16104 (2003).

[44] M. Kratzer and C. Teichert, Nanotechnology **27**, 292001 (2016).

[45] R. Resel, M. Bainschab, A. Pichler, T. Dingemans, C. Simbrunner, J. Stangl, and I. Salzmann, J. Synchrotron Radiat. **23**, 729 (2016).

[46] S. C. B. Mannsfeld and T. Fritz, Mod. Phys. Lett. B **20**, 585 (2006).

[47] D. Nabok, P. Puschnig, C. Ambrosch-Draxl, O. Werzer, R. Resel, and D. M. Smilgies, Phys. Rev. B **76**, 235322 (2007).

[48] K. Hummer, P. Puschnig, and C. Ambrosch-Draxl, Phys. Rev. B **67**, 184105 (2003).

[49] D. Dumcenco, D. Ovchinnikov, K. Marinov, P. Lazić, M. Gibertini, N. Marzari, O. L. Sanchez, Y.-C. Kung, D. Krasnozhon, M.-W. Chen, S. Bertolazzi, P. Gillet, A. Fontcuberta i Morral, A. Radenovic, and A. Kis, ACS Nano **9**, 4611 (2015).

[50] U. Heinemeyer, K. Broch, A. Hinderhofer, M. Kytka, R. Scholz, A. Gerlach, and F. Schreiber, Phys. Rev. Lett. **104**, 257401 (2010).

[51] L. Gisslén and R. Scholz, Phys. Rev. B **80**, 115309 (2009).

[52] V. M. Nichols, K. Broch, F. Schreiber, and C. J. Bardeen, J. Phys. Chem. C **119**, 12856 (2015).

[53] H. Proehl, R. Nitsche, T. Dienel, K. Leo, and T. Fritz, Phys. Rev. B **71**, 165207 (2005).